Synthesis, Electronic Properties, and Applications of Indium Oxide Nanowires

C. LI, D. ZHANG, S. HAN, X. LIU, T. TANG, B. LEI, Z. LIU, AND C. ZHOU

Department of Electrical Engineering–Electrophysics,
University of Southern California, Los Angeles, California, USA

ABSTRACT: Single-crystalline indium oxide nanowires were synthesized using a laser ablation method and characterized using various techniques. Precise control over the nanowire diameter down to 10 nm was achieved by using monodisperse gold clusters as the catalytic nanoparticles. In addition, field effect transistors with on/off ratios as high as 10^4 were fabricated based on these nanowires. Detailed electronic measurements confirmed that our nanowires were n-type semiconductors with thermal emission as the dominating transport mechanism, as revealed by temperature-dependent measurements. Furthermore, we studied the chemical sensing properties of our In_2O_3 nanowire transistors at room temperature. Upon exposure to a small amount of NO_2 or NH_3, the nanowire transistors showed a decrease in conductance of up to five or six orders of magnitude, in addition to substantial shifts in the threshold gate voltage. Our devices exhibit significantly improved chemical sensing performance compared to existing solid-state sensors in many aspects, such as the sensitivity, the selectivity, the response time and the lowest detectable concentrations. We have also demonstrated the use of UV light as a "gas cleanser" for In_2O_3 nanowire chemical sensors, leading to a recovery time as short as 80 seconds.

KEYWORDS: indium oxide; nanowire; transistor; chemical sensor

Recent advances in the field of nanotechnology have led to the synthesis and characterization of a variety of one-dimensional nanostructures, such as semiconductive nanowires.[1–10] These fascinating materials exhibit a variety of interesting properties and may function as the building blocks for nanoscale electronics and nanosensors. Many techniques have been developed to synthesize nanowires, including chemical vapor deposition (CVD),[1–4] laser ablation,[5–7] and electrochemical deposition.[8] These efforts have led to the successful growth of nanowires of various compositions including Ge,[1] ZnO,[2] Si,[4,5] GaN,[6,9] and GaAs,[10] all of which have been employed to function as nanoscale electronic[11] and optoelectronic devices.[12]

Parallel to the success with groups IV and III–V compound semiconductor nanowires, semiconducting oxide nanowires, such as ZnO, CdO, and In_2O_3 are becoming increasingly important. Among them, In_2O_3 is a wide bandgap transparent semiconductor (with a direct band gap of about 3.6 eV and an indirect band gap of about 2.5 eV). In_2O_3 in the bulk form has been widely used in solar cells and organic light emitting diodes.[13,14] More importantly, In_2O_3 films have been demonstrated to work as toxic gas detectors, with detection levels down to 5 ppm for NO_2,[15] due to

Address for correspondence: C. Zhou, Dept. of E.E.-Electrophysics, University of Southern California, Los Angeles, CA 90089, USA.
chongwuz@usc.edu

Ann. N.Y. Acad. Sci. **1006: 104–121 (2003).**
doi: 10.1196/annals.1292.007

the surface interaction and electron transfer between NO_2 molecules and the In_2O_3 surface. In_2O_3 in the nanowire form is expected to offer enhanced sensitivity and also improved response time due to the enhanced surface-to-volume ratios. It is, therefore, important to be able to synthesize In_2O_3 nanowires with highly uniform geometry, preferentially in the single crystalline form, for both electronic property studies and potential sensor applications. Several methods were previously developed to grow In_2O_3 nanowires.[8,16–18] For example, polycrystalline In_2O_3 nanowires were grown by electrodepositing indium into an anodized alumina template with subsequent oxidation.[8] More recently, single crystalline In_2O_3 nanowires were grown by a rapid heating process from indium grains in a mixture of Ar and O_2.[16] However, this method yielded nanowires with a wide diameter distribution due to the lack of a diameter control mechanism. The same is also true for the semiconductive oxide nanobelts reported recently.[17] This drawback can be overcome by using the vapor–liquid–solid (VLS) growth approach,[5] in which the nanowire diameters can be controlled by the catalyst nanoparticle size. An alternative method, based on a template-assisted approach using mesoporous silica also holds great promise for producing single-crystalline In_2O_3 nanowires with uniform morphology.[18] Here, we report an efficient route for the synthesis of single crystalline In_2O_3 nanowires via the vapor–liquid–solid mechanism, in which the In vapor is generated by laser ablation of an indium containing target. Excellent diameter control over the nanowire synthesis was achieved by using monodisperse gold clusters as the catalyst. Transport studies on field effect transistors (FETs) based on individual In_2O_3 nanowires revealed pronounced gate dependence and well-defined linear and saturation regimes that had only previously been observed in conventional silicon metal-oxide–semiconductor FETs and carbon nanotube transistors.[19,20] Thermal emission was determined to be the dominating transport mechanism by temperature dependent measurements. More importantly, In_2O_3 nanowire transistors have been demonstrated to work as chemical sensors for NO_2 and NH_3 at room temperature. Our devices exhibited far superior performance compared to previously reported results. For instance, our devices exhibited sensitivities (defined as the resistance after exposure divided by the resistance before exposure) of 10^6 for NO_2 and 10^5 for NH_3, values that are four or five orders of magnitude better than results obtained with thin-film based sensors.[15] Response times (defined as time duration for resistance change by one order of magnitude) as short as five seconds for 100 ppm NO_2 and 10 s for 1% NH_3 have also been achieved. In addition, careful characterization has revealed the lowest detectable gas concentrations to be 0.5 ppm for NO_2 and 0.02% for NH_3 using our In_2O_3 nanowire transistors. We have also demonstrated the use of UV light as a "gas cleanser" for In_2O_3 nanowire chemical sensors, leading to a recovery time as short as 80 seconds.

FIGURE 1 A shows the schematic diagram of our laser-assisted chemical vapor deposition system. Details of the setup can be found elsewhere.[21] An InAs target was placed at the upstream end of a quartz tube furnace and the In vapor generated during the laser ablation process was carried downstream by a stream of Ar mixed with 0.02% O_2. A Si/SiO_2 substrate decorated with Au clusters was placed at the downstream end and used to collect the final products. The pressure inside the quartz tube was kept at 220 torr and the temperature was maintained at 770°C during the entire process. Our growth follows the well-known vapor–liquid–solid mechanism. This

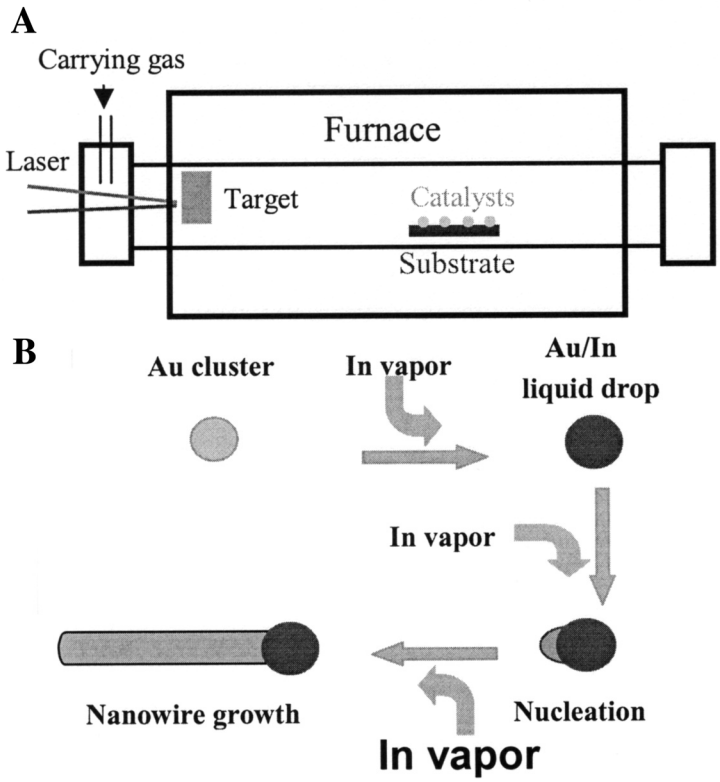

FIGURE 1. A. Schematic diagram of our laser-assisted chemical vapor deposition set-up. **B.** Illustration of the vapor–liquid–solid mechanism. The diameter of the nanowires is directly controlled by the catalyst nanoparticle size.

process is illustrated in FIGURE 1B for our In_2O_3 nanowire growth. Indium atoms in the vapor phase were first alloyed with the gold clusters, and continued supply of indium brought the In/Au solution beyond super-saturation, followed by the out-growth of In and reaction with oxygen at the high temperature to form single crystalline In_2O_3 nanowires. The typical reaction time used was about 35 minutes. After cooling, the samples were characterized using scanning electron microscopy (SEM), X-Ray diffraction (XRD), transmission electron microscopy (TEM), high resolution TEM (HRTEM), and selected area electron diffraction (SAED). The nanowire diameters were usually determined using TEM and the lengths were measured from SEM images.

FIGURE 2A shows a typical SEM image of In_2O_3 nanowires grown on a Si/SiO_2 substrate with evaporated Au thin films as catalysts. These nanowires covered the entire substrate and appeared to be straight. Detailed TEM and SEM examination showed that the nanowires had diameters in the range 30–50 nm and lengths exceeding 3 μm, indicating an aspect ratio of more than 100:1. XRD patterns of such

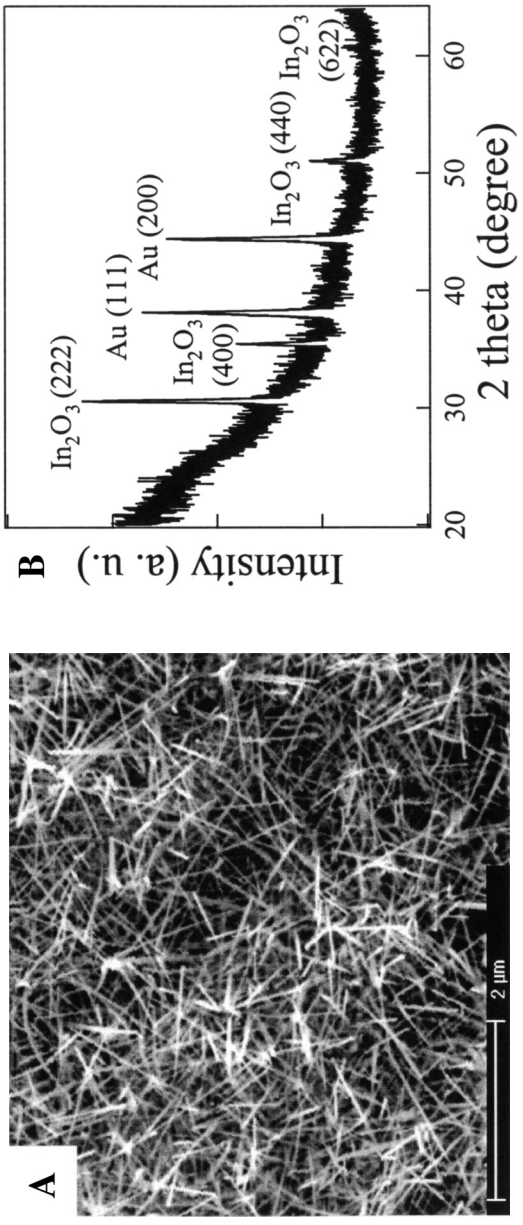

FIGURE 2. **A.** SEM image of In_2O_3 nanowires grown by laser ablation on a Si/SiO_2 substrate coated with 20 Å Au film. **B.** XRD pattern of In_2O_3 nanowires on a Si/SiO_2 substrate. Indices of the peaks are marked above the peaks. Au peaks come from the catalyst.

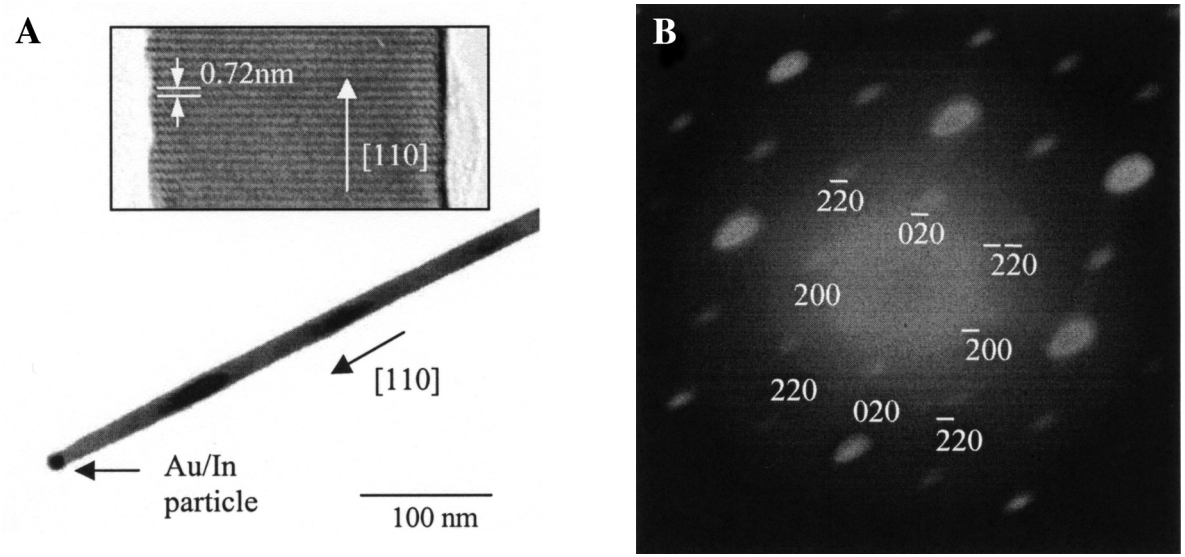

FIGURE 3. A. TEM image of an In_2O_3 nanowire with a catalyst particle at the very tip. The *scale bar* is 100 nm. **Inset**, HRTEM image of an In_2O_3 nanowire showing the [110] growth direction. The lattice spacing is consistent with the lattice constant (10.1 Å) for bulk In_2O_3. **B.** Electron diffraction pattern of the In_2O_3 nanowire indicating the single crystalline nature.

nanowire samples were used to examine the crystal structure of the nanowires. All samples showed similar XRD patterns, indicating the high crystallinity of our nanowires. There are four major diffraction peaks, as shown in FIGURE 2B. They can be indexed to the (222), (400), (440), and (622) crystal planes of a cubic structure of bulk In_2O_3 with a cell constant $a = 1.01$ nm.[22] Two gold peaks from the Au catalysts can also be identified; however, no diffraction peaks from InAs were found in any of our samples. Although this laser ablation process generated both In and As vapors, we believe O_2 is more reactive than As, and hence, In_2O_3 instead of InAs is found to be the final product. Energy dispersive X-ray spectroscopy (EDS) was also performed to analyze the composition of our nanowires: no peaks corresponding to As were detected to the limit of our equipment.

Despite the success mentioned above, direct and precise control over the In_2O_3 nanowire diameter was still required. Furthermore, nanowires with diameters less than 30 nm were also needed in order to make nanowire-based field effect transistors, because of the finite depth to which a gate electric field can penetrate. This was achieved by using monodisperse gold clusters, instead of evaporated gold film, as the catalyst. Three types of cluster were used, with diameters of about 10, 20, and 30 nm. These nanoclusters were dispersed onto a Si/SiO_2 substrate following work published elsewhere[5] and atomic force microscopy (AFM) was performed to confirm that these nanoclusters were distributed uniformly across the surface. Abundant In_2O_3 nanowires were produced all over the substrates using the same laser ablation conditions already described. FIGURE 3A shows a detailed TEM examination of a single In_2O_3 nanowire made from a 10-nm Au cluster. The Au/In alloy particle, with a diameter about 10 nm, can be clearly seen at the tip of the nanowire. The In_2O_3 appeared rather homogeneous without any domain boundaries, indicating the single crystalline nature of our material, as expected from the vapor–liquid–solid growth mechanism. The nanowire diameter (approximately 10 nm) is apparently consistent with the diameter of the catalytic particle. The highly crystalline nature of our In_2O_3 nanowires was further confirmed by selective area electron diffraction. FIGURE 3B shows a SAED pattern, recorded perpendicular to a nanowire long axis. By analyzing the SAED pattern, we estimate that the nanowire adopts a cubic crystal structure with a lattice constant of 1.03 nm, consistent with the lattice constant of bulk In_2O_3 ($a = 1.01$ nm).[22] In addition, by indexing the pattern, we demonstrated that the [110] direction is the nanowire growth direction. A high resolution TEM image is shown in the inset of FIGURE 3A. The lattice spacing along the [110] growth direction (0.72 nm) is in good agreement with the lattice constant for In_2O_3 (1.01 nm). Furthermore, it is apparent from the HRTEM image that there is no native oxide layer outside our nanowire, in sharp contrast to nanowires made from conventional semiconductors, such as Si and InP. This important discrepancy leads to significant results, such as reliable electrical contacts and superior chemical sensing properties, for our In_2O_3 nanowires.

The growth and characterization method mentioned above allowed us to convincingly establish the diameter-controlled growth of In_2O_3 nanowires by using three kinds of Au clusters (10 ± 1.5 nm, 20 ± 2.0 nm, and 30 ± 3.0 nm) as the catalytic particles. FIGURE 4A, C, and E are typical TEM images for In_2O_3 nanowires grown from these clusters. A direct connection between the catalytic particle size and the nanowire diameter is clearly visible. TEM inspection was performed for fifty nanowires

of each kind of gold cluster to generate the wire diameter distribution shown in FIGURE 4B, D, and F. The mean nanowire diameters are 10.9 ± 1.1 nm, 20.6 ± 2.5 nm, and 30.1 ± 2.4 nm, respectively. From these histograms, we can see the width of the nanowires mirrors the colloid catalyst particle size very well.

The ability to produce nanowires of small and uniform diameters is especially important for fundamental studies, such as their electronic properties. In_2O_3 is known to be non-stoichiometric *n*-type semiconductor in the bulk form due to the

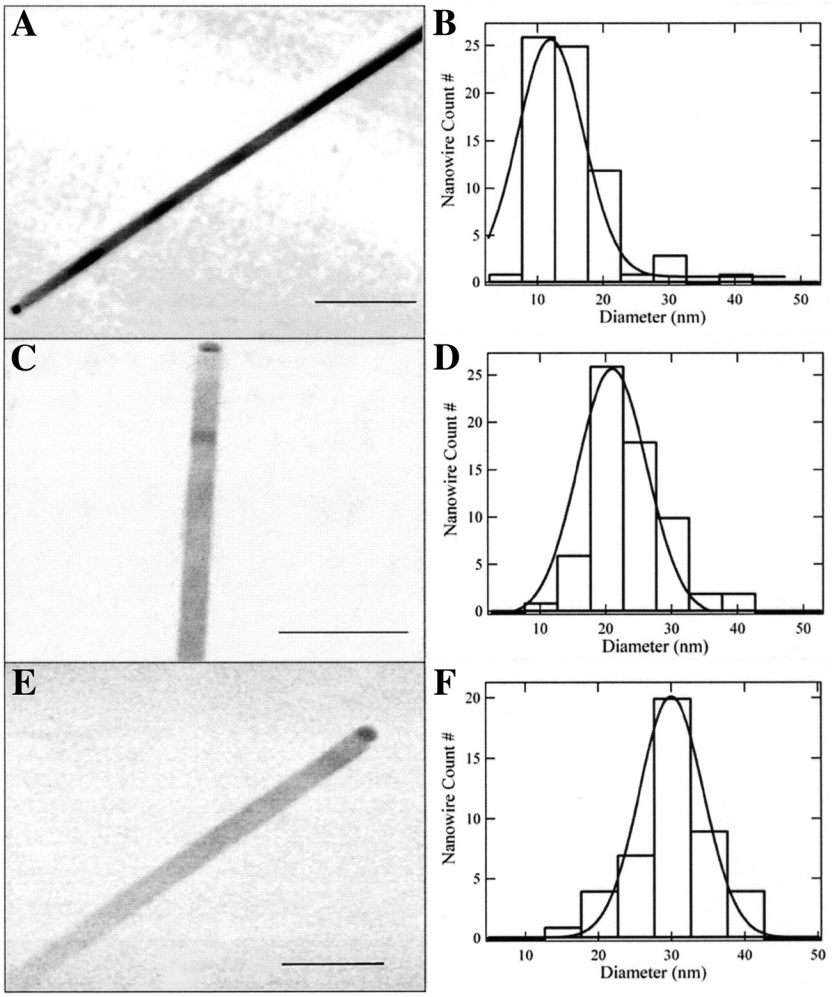

FIGURE 4. TEM images of typical In_2O_3 nanowires grown using monodisperse Au clusters with **(A)** 10 nm, **(C)** 20 nm, and **(E)** 30 nm diameter. *Scale bars* are 100 nm for all three images. Corresponding histograms for the nanowire diameter distributions are plotted in **(B)**, **(D)**, and **(F)**, respectively. The *solid lines* correspond to Gaussian fits.

oxygen vacancies.[15] To our best knowledge, we have made the first In_2O_3 nanowire field effect transistors. A degenerately doped silicon wafer covered with 500 nm SiO_2 was used as the substrate on which In_2O_3 nanowires of various diameters were deposited. Photolithography was performed, followed by evaporating Ti/Au to contact both ends of the nanowires. A typical SEM image of our device is shown in FIGURE 5A (upper inset), indicating a channel length of 3 μm between the source and drain electrodes. The silicon substrate was used as a back gate. We have tested transistors based on nanowires of various diameters and it has been consistently observed that nanowires with larger diameters exhibited weaker gate dependence and lower transconductance, as a result of the finite penetration depth of the gate electric field. In what follows we focus on devices made with nanowires of about 10 nm diameter. FIGURE 5A shows a typical FET I–V_{ds} characteristic curve of the device at room temperature. Six I–V_{ds} curves at V_g = 15, 10, 7, 0, −7, and −10 V are displayed in this figure. With the gate voltage varying from +15 V to −10 V, the conductance of the nanowire was gradually suppressed. From the slopes of the I–V_{ds} curves at $V_{ds} = 0$ V, we observe that the derivative conductance of the In_2O_3 nanowire at this bias was reduced from 3.13×10^{-6} S at V_g = 15 V to 3.62×10^{-10} S at $V_g = -10$ V. In the positive drain–source bias region, the device was almost fully depleted at $V_g = -7$ V and $V_g = -10$ V. This behavior agrees with the well-known fact that In_2O_3 is an *n*-type semiconductor, due to the oxygen vacancies. More interestingly, all the I–V_{ds} curves exhibited asymmetric features with respect to the bias voltage. A case in point is the curve recorded at $V_g = 0$ V. The current changes linearly with V_{ds} in the negative bias region, and reaches saturation when V_{ds} is greater than 0.1 V. A similar phenomenon was observed for *p*-type carbon nanotube transistor devices.[19,20] This saturation behavior is similar to the pinch-off effect in conventional silicon FETs. More information about this *n*-type transistor can be obtained from the I–V_g curve shown in the lower-right inset. The curve was taken at $V_{ds} = 0.32$ V, the current drops dramatically from 6.54×10^2 nA at V_g = 14 V to 3.15×10^{-2} nA at $V_g = -9$ V, indicating an on/off ratio of 2.08×10^4. We take $V_t = -9$ V as the threshold voltage necessary to completely deplete the nanowire; the carrier concentration along the wire can be estimated using the formula $n = Q/eL = 2\pi\varepsilon\varepsilon_0 V_t/[e \ln(2h/r)]$,[23] where Q is the charge, e is the electron charge, ε_0 is the vacuum dielectric constant, L and r are the length and radius of the nanowire, h the thickness of the SiO_2 layer, and ε is the relative dielectric constant. We then calculate the value of n to be 2.30×10^7 cm^{-1} by substituting the data $V_t = -9$ V, r = 5 nm, h = 500 nm, and ε = 3.9. The mobility of the carriers can be obtained from the equation: $dI/dV_g = n\mu e V_{ds}/V_t L$. We obtain $\mu = 98.1$ cm^2/Vsec with V_{ds} = 0.32 V, L = 2 μm, and $dI/dV_g = 6.42 \times 10^{-8}$ A/V. This mobility value compares well with a mobility of 3.17 cm^2/Vsec reported for B-doped Si nanowires,[24] indicating the high quality of our nanowires.

To further explore the electronic properties of the In_2O_3 nanowire device, we measured the I–V curves as a function of temperature, as shown in FIGURE 5B. These I–V curves were taken at 290, 180, 120, 70, 30, and 10 K, with 0 V applied to the gate electrode. The conductance of this device decreases monotonically by several orders of magnitude as the temperature decreases and a gap at about zero bias can be clearly seen for I–V curves taken at 30 K. FIGURE 5B (inset) shows a plot of the zero-bias conductance versus $1/T$, where the dots indicate experimental data and the solid line is a fit calculated according to $G \approx \exp(-E_a/k_B T)$, with a thermal activation barrier

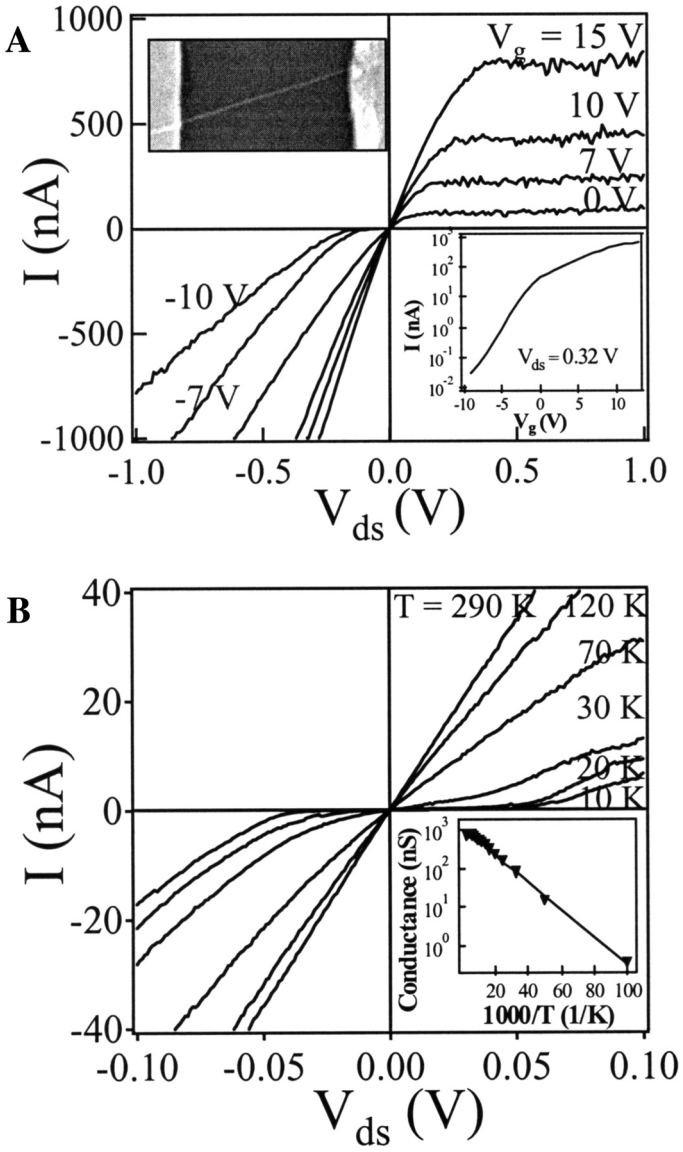

FIGURE 5. A. Gate-dependent *I–V* curves recorded at room temperature. The *lower inset* shows the current versus gate voltage at $V_{ds} = 0.32\,V$. The gate modulated the current by five orders of magnitude. The *upper left inset* is an SEM image of the metal/In_2O_3 nanowire/metal device used for this study. The diameter of the In_2O_3 nanowire is 10 nm and the length between two Ti/Au electrodes is 3 μm. **B.** *I–V* curves obtained at various temperatures at $V_g = 0\,V$. The corresponding temperatures were 290, 180, 120, 70, 30, and 10 K. Suppression of conduction around zero bias was observed in the curves for $T = 20\,K$ and $T = 10\,K$. **Inset**, conductance (logarithmic scale) versus inverse temperature ($1/T$).

$E_a \approx 6.90$ meV. This indicates that the transport through our device was dominated by thermal activation of electrons across the metal–semiconductor Schottky barriers. The barrier height of 6.90 meV was sufficiently low to produce ohmic behavior at room temperature; however, below a temperature of 20 K, where $k_BT < E_a$, thermally activated transport through the system was quenched and, therefore, a gap appeared in the small bias region near $V_{ds} = 0$ V. At $T = 10$ K, for example, a gap between $V_{ds} = -40$ mV and 50 mV was observed and the sample was virtually insulating within this region under a zero gate bias. Larger $|V|$ brought the device into a conductive state again. Electron transport here is suggested to be dominated by the quantum-tunneling effect. Similar mechanisms are reported elsewhere.[19]

Our nanowire chemical sensing measurements were based on these In_2O_3 nanowire transistors. The devices were mounted in a small chamber with electric feedthrough. The system was usually first pumped to vacuum to clean up the surface of the nanowires, and then the conductance of the nanowires was monitored while flowing diluted NO_2 (0.5 to 100 ppm) or NH_3 (0.02% to 1%) in Ar or dry air. FIGURE 6A shows *I–V* curves recorded before and after exposing the nanowire device to 100 ppm NO_2 in Ar for five minutes with 0 V applied to the gate electrode. Different scales (left axis for the curve before the exposure and right axis for the curve after the exposure) were used to elucidate the change in current magnitude. The *I–V* curve recorded before the exposure is typical of our In_2O_3 nanowire field effect transistors with a well-defined linear regime and a saturation regime under a positive bias. The zero-bias resistance for this device was 580 kΩ. After the exposure the device showed a reduction in conductance about six orders of magnitude for $V_{ds} = 0.3$ V, as manifest in the data shown in FIGURE 6A. We also found that, within the NO_2 concentrations (0.5 to 100 ppm) we tested, the conductance of the nanowire transistor always decreased after the exposure and eventually saturated at a level similar to the curve shown in FIGURE 6A, although longer response time was observed for lower concentrations. After each exposure, the system was pumped to vacuum, followed by UV illumination to desorb the NO_2 molecules. The device fully recovered to its initial status immediately after the UV was turned on. Careful analysis of the response of the device under UV illumination reveals a recovery time less than 30 seconds. The underlying physics is that UV exposure generates electron and hole pairs in the nanowire and the adsorbed NO_2 molecules undergo a transition from NO_2^- to NO_2 by taking one hole and then leaving the nanowire surface. This recovery mechanism works for all sorts of adsorbed species, such as NO_2, NH_3, O_2, and moisture and we used it throughout our study to bring the device to its initial state after each exposure.

FIGURE 6B shows two curves recorded before and after the NH_3 exposure with the gate bias maintained at −30 V. A reduction in conductance of five orders of magnitude for $V_{ds} = -0.3$ V was obtained. Our sensitivity values (10^6 for NO_2 and 10^5 for NH_3) are significantly higher than previously reported for NO_2 and NH_3 sensing. For example, typical thin-film based chemical sensors exhibited sensitivities of 58% for NO_2 and 15% for NH_3,[15] whereas sensitivities of less than 100 were obtained for NO_2 using SnO_2 nanobelts.[25] The maximum sensitivities obtained from semiconducting nanotubes were 1,000 for NO_2 and 100 for NH_3.[26] The enhanced sensitivity with our devices is primarily attributed to the enhanced surface-to-volume ratio due to the small diameter (10 nm) of our nanowires, as compared to thin films and SnO_2 nanobelts (typically 80–120 nm in width and 10–30 nm in thickness).[15,25,27]

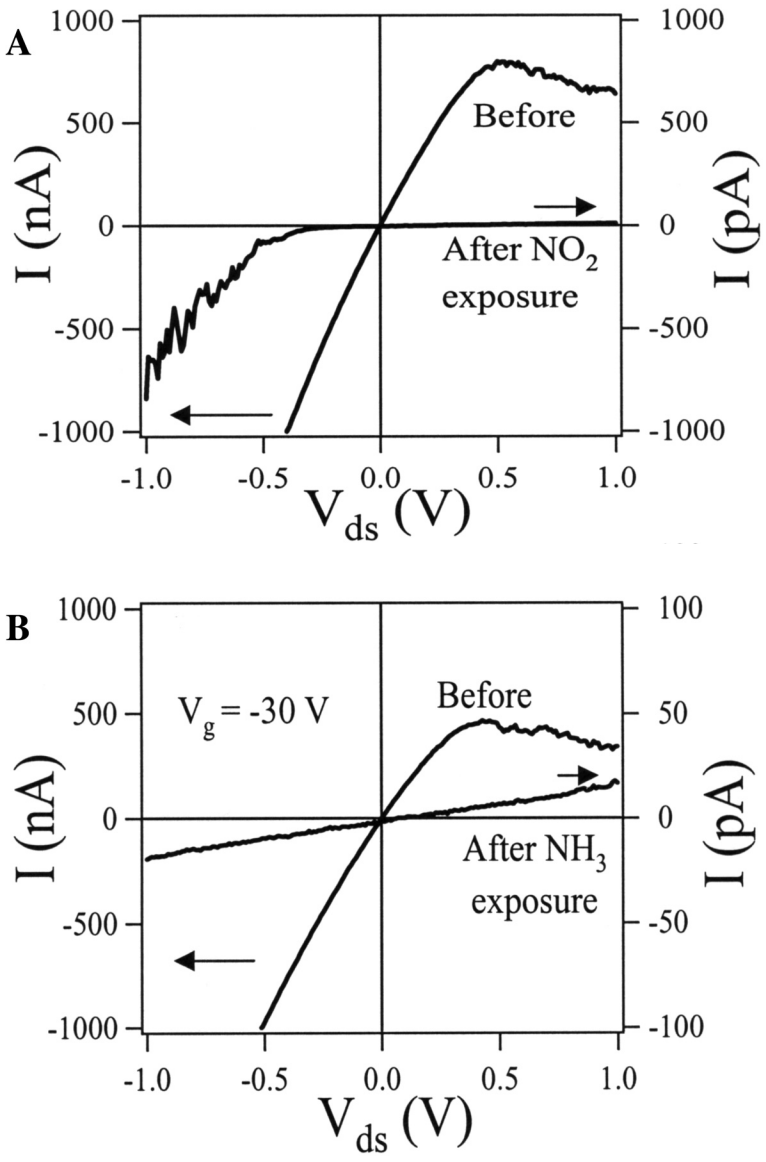

FIGURE 6. A. *I–V* curves measured before and after exposure to 100 ppm NO_2. **B.** *I–V* curves measured before and after exposure to 1% NH_3 with $V_g = -30$ V. The *arrows* indicate different scales used for the curves.

An additional reason is related to the nature of the In_2O_3 nanowire surface, which can readily react with ambient species, in comparison with the inert sidewall of carbon nanotubes.[26]

The sensing properties of our devices can also be studied by monitoring the current dependence on gate bias, rendering a significant advantage over thin-film based devices.[15] FIGURE 7A shows two I–V_g curves recorded before and after exposure to 100 ppm NO_2 in argon with a constant $V_{ds} = -0.3$ V. Both curves confirm that In_2O_3 nanowires are *n*-type doped semiconductors, as indicated by the reduced conductance under negatively increasing gate bias. However, a striking feature in FIGURE 7A

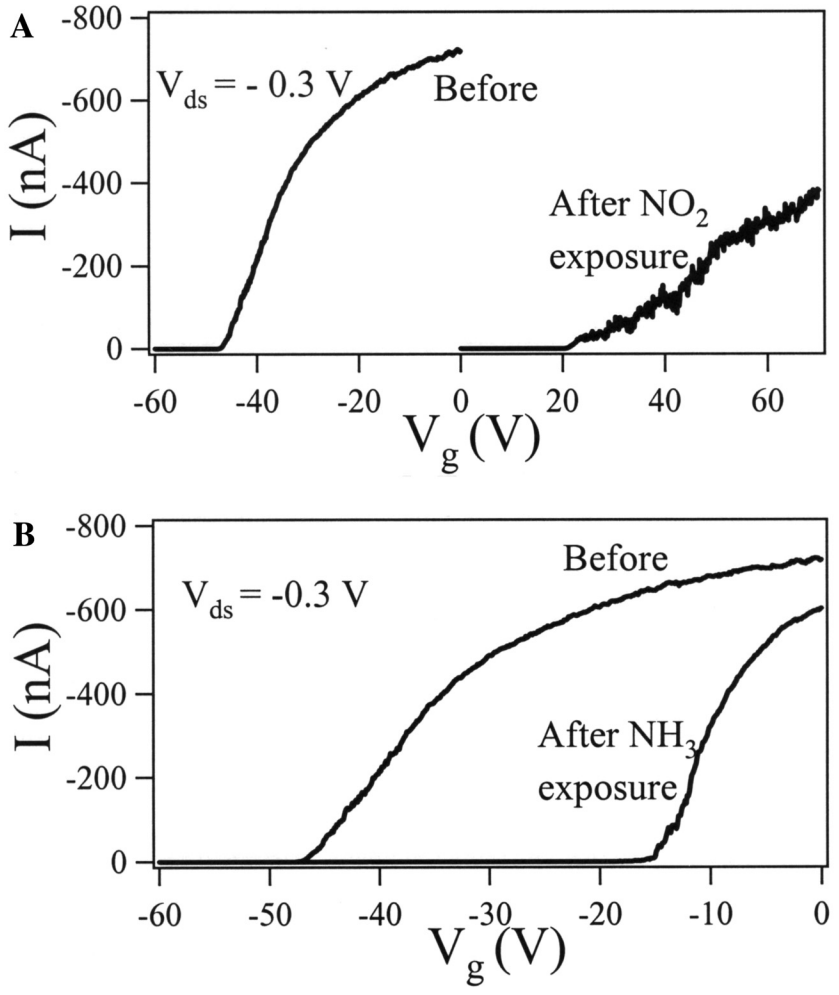

FIGURE 7. A. I–V_g curves before and after exposure to 100 ppm NO_2 with $V_{ds} = -0.3$ V. **B.** I–V_g curves before and after exposure to 1% NH_3 with $V_{ds} = -0.3$ V.

is a pronounced shift in the threshold voltage from −48 V before the exposure to 20 V after the exposure. The response to NO_2 can be understood by considering the interaction between NO_2 and the *n*–type doped In_2O_3 nanowires. Adsorption of oxidizing gases (such as NO_2) reduces the number of free electrons in the material and, thus, reduces the conductivity. The change of carrier concentration after NO_2 exposure can be estimated to be $C\Delta V_t/eL \approx 1.72 \times 10^8 \text{cm}^{-1}$, where ΔV_t is the shift in the threshold voltage and C is the capacitance of nanowire, estimated to be 1.21×10^{-16}F.[23] This indicates adsorption of about 17 NO_2 molecules per nanometer if we assume each adsorbed molecule takes one electron away from the nanowire. Our results further point out the possibility of single molecule detection by using In_2O_3 devices with ultrashort channel length (a few nanometers).

FIGURE 7B shows two I–V_g curves before and after exposing the device to diluted NH_3 in Ar with $V_{ds} = -0.3$ V. A significant shift in the threshold voltage from −48 V to −16 V was observed, with maximum sensitivity 10^5 near $V_g = -30$ V. Our results are qualitatively different from previously published results based on In_2O_3 thin films operating at elevated temperatures (450°C),[15] where an enhancement of the conduction was observed. Since UV illumination was used in our study before NH_3 exposure to desorb the attached molecules on the In_2O_3 nanowire surface, our results suggest that NH_3 might adsorb as an electron-withdrawing species on clean *n*-type doped In_2O_3 nanowires. More experimental work, as well as theoretical investigation, is necessary for better understanding. An important consequence of the gate dependent measurements is that selectivity between different gas species can be achieved by comparing the shift in the threshold voltage. Our measurements have shown that NO_2 of various concentrations consistently shifted the threshold voltage to around 20 V, whereas NH3 of various concentrations consistently shifted the threshold voltage to about −16 V. This can be understood, since the final threshold voltage is directly related to the electron transfer between the nanowire and the adsorbed molecules and, thus, can be used to pinpoint one chemical among similar species.

As well as the sensitivity, two other important parameters for chemical sensors are the response time and the lowest detectable concentrations for toxic species. The In_2O_3 nanowire sensors also showed advantages in these aspects. FIGURE 8A shows the response of the In_2O_3 nanowire device to 100 ppm, 2 ppm, and 0.5 ppm NO_2 in Ar with $V_g = 0$ V and $V_{ds} = 0.3$ V. The current was observed to decrease sharply to almost zero within 50 seconds after exposure to 100 ppm NO_2. Detailed analysis revealed a response time (defined as the time for the conductance to change by one order of magnitude) of less than five seconds for 100 ppm NO_2, about five minutes for 2 ppm NO_2, and about 10 minutes for 0.5 ppm NO_2, as shown in FIGURE 8A. This is significantly better than the response time of 50 sec for thin-film based semiconducting oxide sensors operating at elevated temperatures upon exposure to 100 ppm NO_2.[28] The lowest detectable concentration of NO_2 has been determined to be 5 ppb in our recent experiments.

Similar measurements were carried out to determine the response time to NH_3, where we applied a gate voltage of −30 V with a constant source-drain bias of −0.3 V. The conductance of the In_2O_3 nanowire was observed to decrease by five orders of magnitude after exposure to 1% NH_3 within 30 sec, as shown in FIGURE 8B. The response time corresponding to a ten-fold decrease was determined to be less than

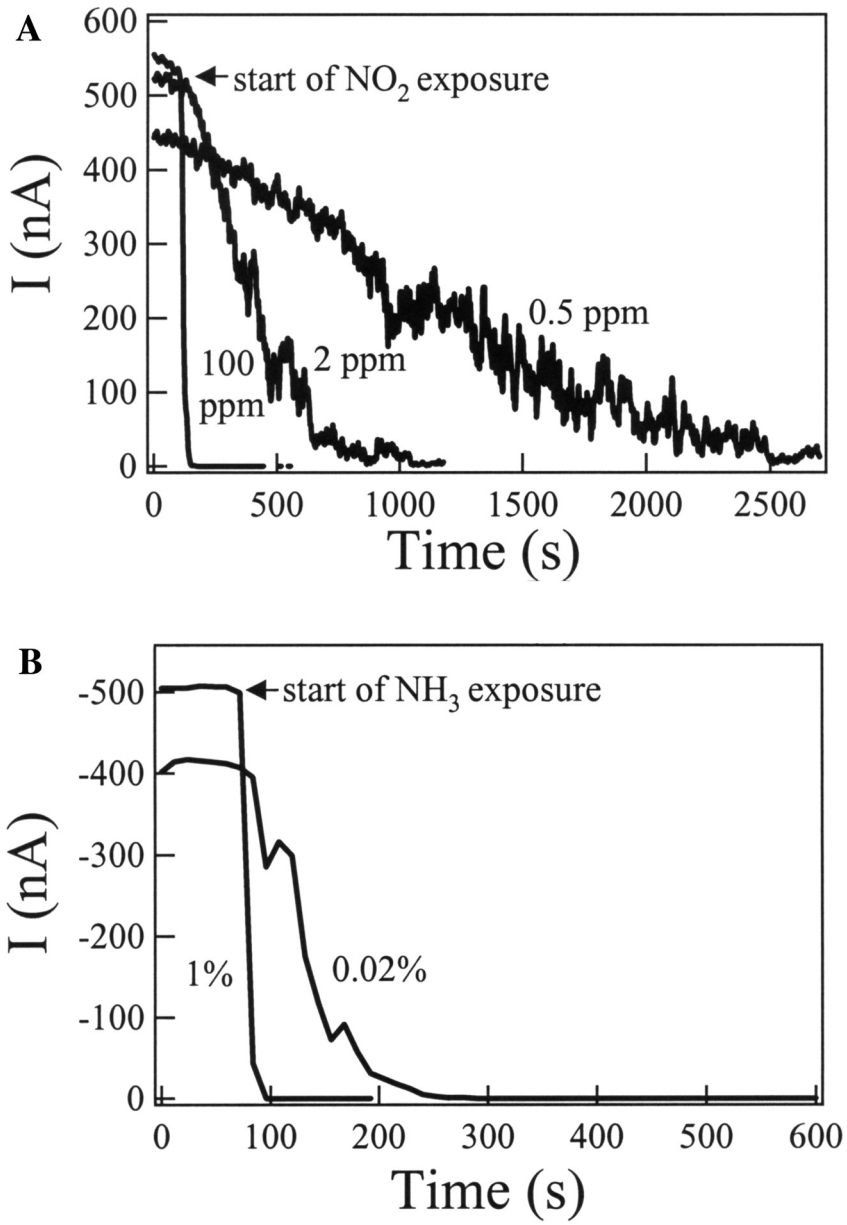

FIGURE 8. Response of the In_2O_3 nanowire sensor to various NO_2 concentrations **(A)** and NH_3 concentrations **(B)**. These reveal a response time less than five seconds for 100 ppm NO_2 and less than 10 seconds for 1% NH_3.

10 seconds. For comparison, the response times to 1% NH_3 for single-walled semiconducting carbon nanotubes is about 1–2 min, and the sensitivity is only 10–100.[26] The lowest concentration for NH_3 we tested was 0.02%, where the limitation was imposed by the availability of highly diluted NH_3 in air or argon.

We also used dry compressed air instead of Ar in our sensing experiments and similar results were observed.[29] For instance, after flowing 100 ppm NO_2 mixed in air, the conductance of our nanowire transistor decreased by one order of magnitude within 30 sec and the threshold gate voltage shifted by 50 V. Overall, the oxygen molecules in the compressed air showed rather minor influence and the effects of NO_2 and NH_3 can be clearly distinguished.

Inspired by the interaction between UV light and the nanowires, we tried using UV light as a "cleanser" for our In_2O_3 nanowire gas sensors.[30] Since the UV light can efficiently desorb ambient gas molecules from the nanowire surface, a short recovery time for the gas sensors was expected. FIGURE 9 shows a current versus time curve we recorded with the nanowire device mounted in a sealed chamber. The device was biased at 0.05 V with the gate electrode fixed at 0 V. The chamber was pumped to high vacuum before the measurement. The current maintained a constant level (13.5 nA) until the device was exposed to 254 nm UV light (point *a*), and then rose rapidly during the illumination. We turned off the lamp at $t = 200$ sec (point *b*) and turned on Ar gas flow simultaneously. This led to a small decrease in the current

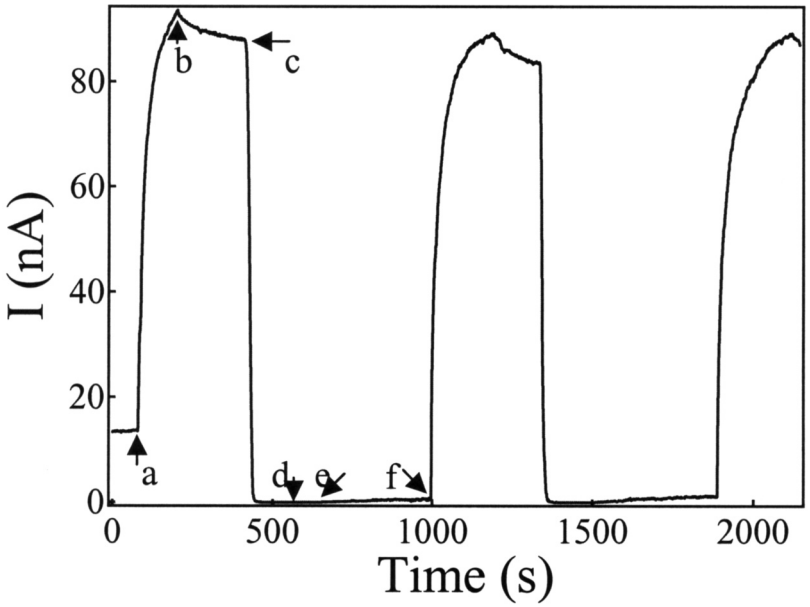

FIGURE 9. Two NO_2 gas sensing cycles. Point *a*, the 254 nm UV light was turned on; *b*, the UV light was turned off and the Ar gas flow was turned on at the same time; *c*, 0.1% NO_2 gas was added to the pure Ar flow; *d*, the NO_2 supply was stopped; *e*, the Ar flow was turned off and the system was evacuated; *f*, the UV light was turned on.

due to the recombination of electrons and holes. 0.1% NO_2 gas was added to the pure Ar flow at point *c*. The current showed a sharp decrease upon the exposure to NO_2, because NO_2 can adsorb on the nanowire surface and withdraw electrons from the nanowire to form NO_2^-. We stopped the NO_2 supply at 600 sec (point *d*), and then turned off Ar flow and pumped the system at 700 sec (point *e*). However, as shown in the figure, neither Ar flow nor pumping can desorb the NO_2 molecules adsorbed on the nanowire surface in an effective manner and the device remained in the highly resistive state. To effectively recover the sensor, we turned on the UV lamp again at point *f*. The UV light illumination immediately brought the device back to the high conductive state. We repeated this process (from *b* to *f*) again. The highly reversible behavior of the device is explicitly shown in FIGURE 9. The application of UV light significantly shortened this "cleaning" process and reduced the recovery time of the sensor to only 80 sec. This example perfectly reveals the light-enhanced desorption kinetics in the nanowire systems.

In conclusion, high-quality indium oxide nanowires were synthesized using a laser ablation technique. Their composition and single crystalline structure were confirmed using XRD, TEM, and SAED. Precise control over the nanowire diameter was achieved by using monodisperse gold clusters as the catalytic nanoparticles. The growth can be explained by the VLS mechanism. Field effect transistors were fabricated based on these nanowires. Detailed electrical measurements confirmed that the indium oxide nanowires were *n*-type semiconductors and exhibited nice transistor characteristics with well-defined linear and saturation regimes. On/off ratios as high as 2.08×10^4 and an electron mobility of 98.1 cm^2/Vsec were observed in air at room temperature. Temperature-dependent measurements revealed thermal emission as the dominant transport mechanism with an activation barrier of 6.90 meV. In addition, In_2O_3 nanowires have been demonstrated to work as chemical sensors at room temperature. Our devices showed sensitivities as high as 10^6 for diluted NO_2 and 10^5 for diluted NH_3. Substantial shifts in the threshold voltage were also observed and can be used to distinguish various gas species. The response times were determined to be five seconds for 100 ppm NO_2 and 10 sec for 1% NH_3, and the lowest detectable concentrations were 5 ppb for NO_2 and 0.02% for NH_3. Our work clearly demonstrates the advantages of nanowire as a building block for nanoelectronics in the near future.

ACKNOWLEDGMENTS

The authors thank Dr. Jie Han and Dr. Meyya Meyyapan at NASA Ames Research Center for valuable technical discussions. Professor Edward Goo and the USC Microscope Center are acknowledged for the use of their facilities. We thank Professor Martin Gundersen and Dr. Xiaodong Zhang for their help with the laser ablation process. This work is supported by USC, a Powell award, NASA contract NAS2-99092, NSF CAREER award, NSF NER program, and a Zumberger award.

REFERENCES

1. WU, Y. & P. YANG. 2000. Germanium nanowire growth via simple vapor transport. Chem. Mater. **12:** 605–607.
2. HUANG, M.H., *et al.* 2001. Catalytic growth of zinc oxide nanowires by vapor transport. Adv. Mater. **13:** 113–116.
3. KONG, J., *et al.* 1999. Synthesis, integration, and electrical properties of individual single-walled carbon nanotube. Appl. Phys. A **69:** 305–308.
4. CUI, Y., *et al.* 2001. Diameter-controlled synthesis of single-crystal silicon nanowires. Appl. Phys. Lett. **78:** 2214–2216.
5. HU, J., *et al.* 1999. Chemistry and physics in one dimension: synthesis and properties of nanowires and nanotubes. Acc. Chem. Res. **32:** 435–445.
6. DUAN, X. & C.M. LIEBER. 2000. Laser-assisted catalytic growth of single crystal GaN nanowires. J. Am. Chem. Soc. **122:** 188–189.
7. MORALES, A.M. & C.M. LIEBER. 1998. A laser ablation method for the synthesis of crystalline semiconductor nanowires. Science **279:** 208–211.
8. ZHENG, M., *et al.* 2001. Ordered indium-oxide nanowire arrays and their photoluminescence properties. Appl. Phys. Lett. **79:** 839–841.
9. CHEN, C. & C. YEH. 2000. Large-scale catalytic synthesis of crystalline gallium nitride nanowires. Adv. Mater. **12:** 738–741.
10. DUAN, X. & C.M. LIEBER. 2000. General synthesis of compound semiconductor nanowires. Adv. Mater. **12:** 298–302.
11. HUANG, Y., *et al.* 2001. Logic gates and computation from assembled nanowire building blocks. Science **294:** 1313–1317.
12. HUANG, M., *et al.* 2001. Room-temperature ultraviolet nanowire nanolasers. Science **292:** 1897–1899.
13. SREENIVAS, K., *et al.* 1985. Preparation and characterization of rf sputtered indium tin oxide films. J. Appl. Phys. **57:** 384–392.
14. SHIGESATO, Y., *et al.* 1992. Electrical and structural properties of low resistivity of low resistivity tin-doped indium oxide films. J. Appl. Phys. **71:** 3356–3364.
15. LIESS, M. 2002. Electric field-induced migration of chemisorbed gas molecules on a sensitive film—a new chemical sensor. Thin Solid Films **410:** 183–187.
16. PENG, X., *et al.* 2002. Synthesis and photoluminescence of single-crystalline In_2O_3 nanowires. J. Mater. Chem. **12:** 1602–1605.
17. PAN, Z., *et al.* 2001. Nanobelts of semiconducting oxides. Science **291:** 1947–1949.
18. YANG, H., *et al.* 2003. One-step nanocasting synthesis of highly ordered single crystalline indium oxide nanowire arrays from mesostructured frameworks. J. Am. Chem. Soc. **125:** 4724–4725.
19. ZHOU, C., *et al.* 2000. Electrical measurements of individual semiconducting single-walled carbon nanotubes of various diameters. Appl. Phys. Lett. **76:** 1597–1599.
20. LIU, X., *et al.* 2001. Carbon nanotube field-effect inverters. Appl. Phys. Lett. **79:** 3329–3331.
21. LI, C., *et al.* 2003. Diameter-controlled growth of single-crystalline In_2O_3 nanowires and their electronic properties. Adv. Mater. **15:** 143–146.
22. WYCKOFF, R.W.G. 1968. Crystal Structures. Interscience, New York.
23. MARTEL, R., *et al.* 1998. Single- and multi-wall carbon nanotube field-effect transistors. Appl. Phys. Lett. **73:** 2447–2449.
24. CUI, Y., *et al.* 2000. Doping and electrical transport in silicon nanowires. J. Phys. Chem. B **104:** 5213–5216.
25. COMINI, E., *et al.* 2002. Stable and highly sensitive gas sensors based on semiconducting oxide nanobelts. Appl. Phys. Lett. **81:** 1869–1871.
26. KONG, J., *et al.* 2000. Nanotube molecular wires as chemical sensors. Science **287:** 622–625.
27. LAW, M., *et al.* 2002. Photochemical sensing of NO_2 with SnO_2 nanoribbon nanosensors at room temperature. Angew. Chem. Int. Ed. **41:** 2405–2408.
28. SHIMIZU, Y. & M. EGASHIRA. 1999. Basic aspects and challenges of semiconductor gas sensors. MRS Bull. **24:** 18–24.

29. LI, C., *et al.* 2003. Surface treatment and doping dependence of In_2O_3 nanowires as ammonia sensors. J. Phys. Chem. B. In press.
30. ZHANG, D., *et al.* 2003. Ultraviolet photodetecting properties of indium oxide nanowires. Appl. Phys. A **77:** 163–166.